

# Particle-in-cell simulation of ion beam extraction from a pulsed plasma through a grid

Sang Ki Nam, Demetre J Economou and Vincent M Donnelly

Plasma Processing Laboratory, Department of Chemical and Biomolecular Engineering,  
University of Houston, Houston, TX 77204-4004, USA

Received 24 May 2006, in final form 2 November 2006

Published 24 November 2006

Online at [stacks.iop.org/PSST/16/90](http://stacks.iop.org/PSST/16/90)

## Abstract

A particle-in-cell simulation with Monte Carlo collisions was developed to study ion extraction from a capacitively-coupled argon plasma through a grid. A one-dimensional simulation of the plasma reactor was coupled with a two-dimensional simulation of the sheath region over a grid hole. The 13.56 MHz power applied to the plasma was pulsed 50  $\mu\text{s}$  ON and 50  $\mu\text{s}$  OFF. A dc bias voltage was applied in the afterglow (power OFF fraction of the cycle), to raise the plasma potential and expel ions out of the plasma through the grid. The electron temperature decayed rapidly in the afterglow, minimizing spatial variations of the plasma potential and allowing a nearly mono-energetic ion beam to be extracted. Due to the absence of plasma moulding over the grid holes, the beam was highly directional with an angular spread decreasing with increasing dc bias. The applied dc bias also set the beam energy. Simulation predictions were in good quantitative agreement with measurements. The ion beam could be neutralized by grazing angle collisions on a set of parallel neutralization plates downstream of the extraction grid, to produce a highly directional and nearly mono-energetic neutral beam.

## 1. Introduction

Precise control of the ion energy distribution (IED) is important in a variety of thin film etching and deposition applications [1]. In plasma processing, for example, etch rate and selectivity depend sensitively on ion bombardment energy, especially for near-threshold processes. In nano-pantography, a massively parallel technique to fabricate nanometre-sized patterns over large areas [2], a collimated, mono-energetic ion beam is essential. For ion beams extracted from plasma sources, the IED is determined by the difference in potential between the plasma and the substrate, as well as ion collisions with the background neutral gas. For radio frequency (RF) plasmas, commonly employed in semiconductor manufacturing, the dependence of IED on control parameters has been studied [3, 4]. For collisionless ion flow, the ion energy spread depends critically on the ion transit time through the sheath compared with the period of the applied field and the sheath potential waveform [5–7]. Some researchers [8, 9] reported a method to control the ion bombardment energy by applying

a non-sinusoidal bias waveform on the substrate electrode, designed to yield a narrow energy spread. Others [10, 11] showed that ion energy can be controlled by biasing a separate electrode immersed in the plasma to control the plasma potential. This technique was also used to control the energy of ions which were then neutralized to become fast neutrals in neutral beam applications [12, 13].

In all the experiments mentioned above, ions were extracted from a continuous wave (CW) plasma. In a CW plasma, even when the sheath potential waveform is designed to yield a narrow IED, the ion energy spread is limited by the *spatial* variation of the plasma potential. This in turn is proportional to the electron temperature,  $T_e$  [14]. Thus, the energy of an ion entering the sheath depends on *where* the ion was born, and the spread of the resulting IED could be several times  $T_e$ . A way to sharpen the IED is to extract ions from a plasma of very low  $T_e$ .

A nearly mono-energetic ion beam was extracted from a capacitively-coupled, pulsed Ar plasma [15]. The electron temperature decayed rapidly in the afterglow, resulting in

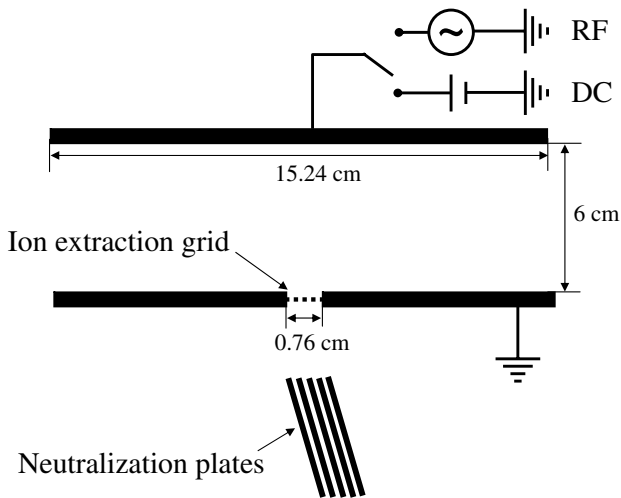


**Figure 1.** Schematic of a capacitively-coupled plasma reactor (not to scale). Radio frequency power (during plasma ON) or a dc bias voltage (during plasma OFF) is applied to the upper electrode. The lower electrode with the ion extraction grid was always grounded. A set of parallel plates (optional) is also shown downstream of the grid to neutralize extracted ions.

nearly uniform plasma potential and minimal energy spread of ions extracted in the afterglow. Ion energy was controlled by a dc bias on an electrode in contact with the plasma. Langmuir probe measurements indicated that this dc bias simply raised the plasma potential without heating the electrons in the afterglow. The energy spread of the extracted ion beam was about an order of magnitude narrower than that extracted from a CW plasma.

In this work a particle-in-cell simulation with Monte Carlo collisions (PIC–MC) was developed to study ion beam extraction from a pulsed plasma. A one-dimensional (1D) simulation of an argon plasma reactor was coupled to a two-dimensional (2D) simulation of the sheath region over the extraction grid. Emphasis was placed on the energy and angular distributions of the extracted ion beam for different applied dc bias voltages in the afterglow of the pulsed plasma. Neutralization of the extracted ion beam by grazing angle scattering on a set of parallel plates downstream of the ion source was also simulated to produce nearly mono-energetic and directional neutral beams.

## 2. Simulation model

Plasma production in a parallel plate system and ion extraction through a grounded grid (figure 1) were simulated. The simulation model consisted of two parts: (1) a one-dimensional self-consistent simulation of a parallel plate capacitively-coupled plasma reactor and (2) a two-dimensional self-consistent simulation of the sheath region over a grid hole and ion extraction through the hole. The two parts were coupled in the sense that the results of the first part were used as input for the second part of the simulation. Since the actual system is at least two-dimensional, the 1D plasma reactor simulation models the region around the centreline of the system in figure 1. This is adequate for the purpose of this work since the extraction grid is at the central region of the

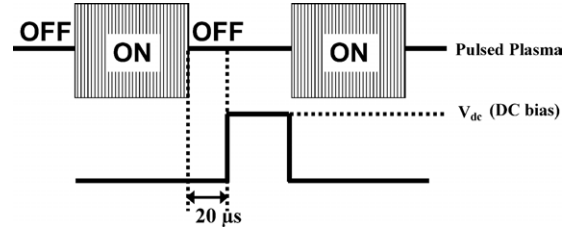


**Figure 2.** A pulsed plasma is created by repeatedly switching radio frequency power ON for  $50 \mu\text{s}$  and OFF for  $50 \mu\text{s}$ .  $20 \mu\text{s}$  into the afterglow (RF power OFF), a dc bias voltage is applied for a set time in the afterglow.

electrode. A separate simulation of ion transport, collision and neutralization on a set of parallel plates downstream of the grid (shown in figure 1) was also performed to evaluate the performance of the system used as a neutral beam source.

### 2.1. Pulsed plasma simulation

A capacitively-coupled parallel plate (plate separation 6 cm) argon plasma reactor was simulated. Radio frequency (RF) power applied to the plasma was pulsed  $50 \mu\text{s}$  ON and  $50 \mu\text{s}$  OFF. During the plasma ON portion of the cycle, a potential  $V = 300 \sin(2\pi ft)$  (in volts, where  $f = 13.56 \text{ MHz}$ ) was applied to the powered electrode while the counter-electrode was grounded (figure 1).  $20 \mu\text{s}$  into the afterglow (RF power OFF), a positive dc bias voltage was applied to the powered electrode (figure 2) to raise the plasma potential and expel ions out of the plasma. The background gas was assumed to be at a uniform density of  $1.9 \times 10^{14} \text{ cm}^{-3}$  (corresponding to 10 mTorr at 500 K). Only argon ions and electrons were considered. Due to the low operating pressure, the effect of metastable ionization on plasma production was neglected. The cross section set for argon gas was obtained from [16]. Energy and angle resolved electron scattering were considered by the method described in [18]. Elastic electron scattering, excitation and ionization as well as ion–neutral collisions were included. Electron–electron collisions were neglected due to the low charge density. The usual restrictions on time step and grid size applied to PIC [17, 18] were observed.

### 2.2. Simulation of the sheath region over a grid hole

A single through hole was used as a simplification of an extraction grid. The hole diameter was  $142 \mu$  and the hole length (or grid thickness) was  $127 \mu$ . The two-dimensional axisymmetric ( $r, z$ ) computational domain (figure 3) extended 3 mm above the hole. The ion density, electron temperature, electron density and RF potential were specified at the top boundary of the computational domain, as given by the 1D pulsed plasma simulation. The wall containing the hole was conductive and at ground potential ( $V = 0$ ). A zero radial potential gradient condition was applied at the perimeter and centreline, while a zero axial potential gradient was applied at the bottom boundary of the computational domain. Only ions were followed by the 2D PIC simulation. The electron density was assumed to be given by the Boltzmann relation. The plasma sheath evolved self-consistently according to the specified conditions. Ions entering at the upper boundary of the computational domain were sampled from the 1D

IED, IAD,  $\Phi$ ,  $N_i$  and  $N_e$  from 1D bulk plasma simulation

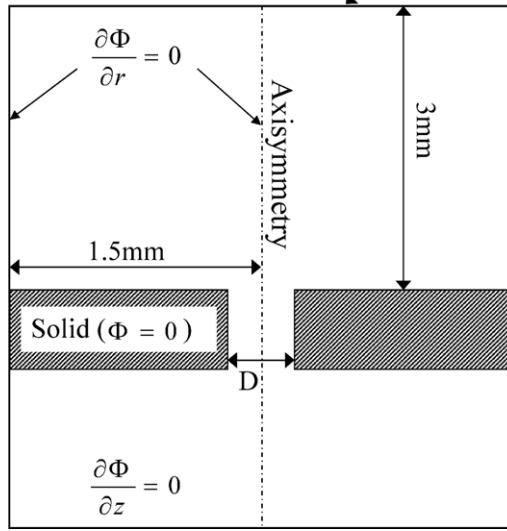


**Figure 3.** The 2D computational domain (not to scale) for ion extraction consisted of an axisymmetric hole through a solid at ground potential, with symmetry condition in the radial direction far from the hole. The ion density, ion velocity distribution, electron density and plasma potential were specified at the top of the domain, as obtained by a 1D PIC–MC plasma simulation.

PIC simulation using the acceptance–rejection method [19]. Computational particles were weighted according to their radial position so that a radially uniform ion flux was injected. An explicit time-centred leap frog method [17] was used for time integration, obeying the Courant condition,  $v\Delta t/\Delta x < 1$ , where  $v$  is the particle speed and  $\Delta t$  and  $\Delta x$  are the time step and grid cell size, respectively. Ion–neutral collisions (elastic scattering and charge exchange) were considered. Particle distribution functions were collected at the bottom boundary of the computational domain. The Poisson equation was solved at each time step using a finite element method. The results shown below were obtained with  $3 \times 10^5$  simulation particles. Energy conservation of the integration scheme was tested using cold ( $T_i = 0$ ) ions in a two-dimensional dc field in the domain of figure 3. All particles collected at the bottom of the computational domain had the same energy, indicating that there were no numerical artefacts.

### 3. Results and discussion

#### 3.1. Plasma properties

Figure 4 shows the time-average electron density (a), effective electron temperature (b) and plasma potential (c) as a function of position between the electrodes during the power ON fraction of the cycle. The effective electron temperature was calculated as  $2/3$  of the average electron energy, the latter found by integrating the electron energy distribution function (EEDF),

$$T_{\text{eff}} = \frac{2}{3} \int \varepsilon f_d(\varepsilon) d\varepsilon, \quad (1)$$

where  $\varepsilon$  is the electron energy (eV) and  $f_d(\varepsilon)$  is a normalized EEDF. The EEDF was found to be similar to that measured

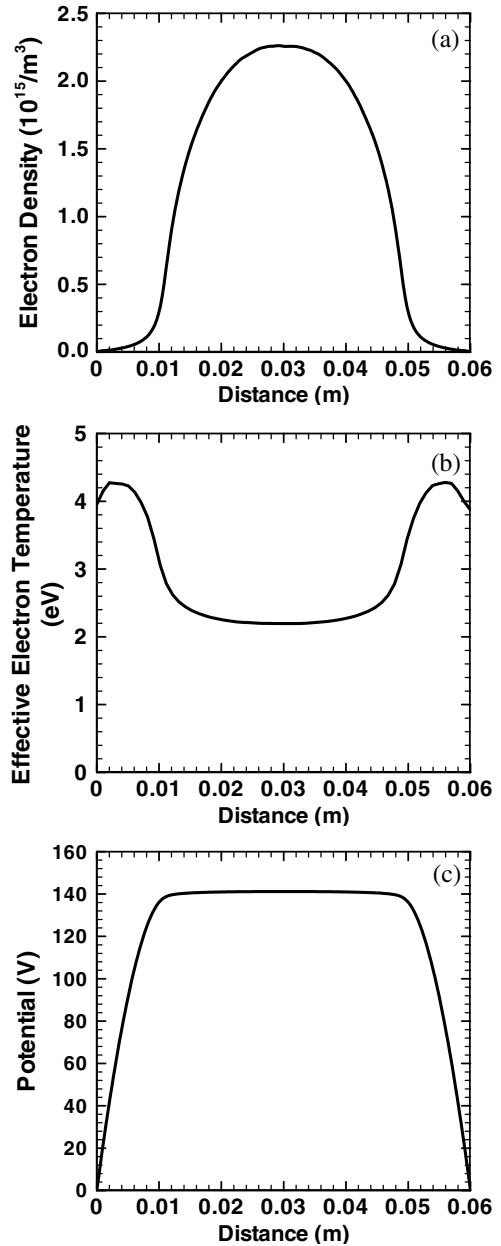


**Figure 4.** Time-average electron density (a), effective electron temperature (b) and potential (c) across the interelectrode gap during the power ON portion of the cycle.

for low pressure capacitively-coupled argon plasmas [20], namely the tail of the distribution is heated by the oscillating sheath. The predicted plasma characteristics of figure 4 are also typical [21]. The electron density (figure 4(a)) peaks at the centre and decays substantially in the 1 cm thick sheaths over each electrode. The effective electron temperature (figure 4(b)) is quite uniform in the bulk plasma, increases near the plasma–sheath interface due to heating by the oscillating sheath and decreases near the wall due to diffusion cooling. The time-average plasma potential indicates that the sheath thickness is about 1 cm. All distributions are symmetric in this one-dimensional system.

Figure 5 shows the time evolution of the electron density and effective electron temperature (at the reactor centre) in

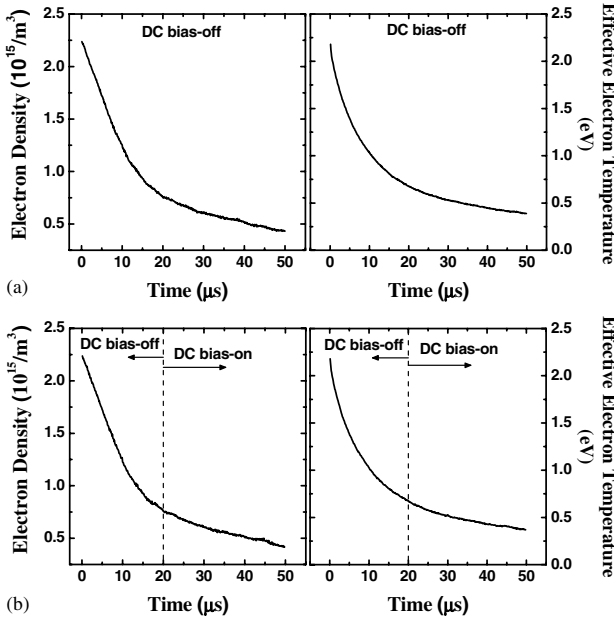


**Figure 5.** Electron density and effective electron temperature at the reactor centre in the afterglow, with no bias applied (a) and with a 50 V dc bias applied 20  $\mu\text{s}$  into the afterglow (b).

the afterglow (after RF power is turned OFF), when no dc bias is applied in the afterglow, (a), and when a 50 V dc bias is applied 20  $\mu\text{s}$  into the afterglow, (b). The electron density decays by about an order of magnitude (by diffusion to the walls), and the electron temperature cools to less than 0.5 eV, 50  $\mu\text{s}$  into the afterglow. Interestingly, the application of a dc bias of 50 V (figure 5(b)) does not alter the decay of electron density and electron temperature in any way (compare (a) with (b)). This indicates that the bias does not heat electrons. The applied dc bias increases the plasma potential, though, as seen in figure 6. Without dc bias applied in the afterglow (figure 6(a)) the plasma potential decays rapidly to zero. When 50 V of dc bias is applied 20  $\mu\text{s}$  into the afterglow (figure 6(b)), the plasma potential rises quickly to the applied bias. This suggests that the application of a dc bias in the afterglow can be used to control the energy of the ions extracted through the grid. It should be noted that the ion energy should equal the plasma potential since the grid is grounded. By changing the applied dc bias the ion energy can be changed at will. Given that the gradients of plasma potential are very small in the afterglow, the extracted ion beam should be quite mono-energetic, assuming that ion-neutral charge exchange collisions do not occur. Figure 7 shows a comparison between simulation predictions (a), with experimental data (b), from [15]. The simulation does a reasonable job of capturing the decay of Ar ion density, electron temperature and plasma potential as measured by a Langmuir probe.

### 3.2. Extracted ion beam properties

The potential distribution around the grid hole 45  $\mu\text{s}$  into the afterglow with a 50 V dc bias applied is shown in Figure 8. Plasma moulding is minimal since the sheath thickness is much larger than the hole diameter [22, 23]. Hence ions

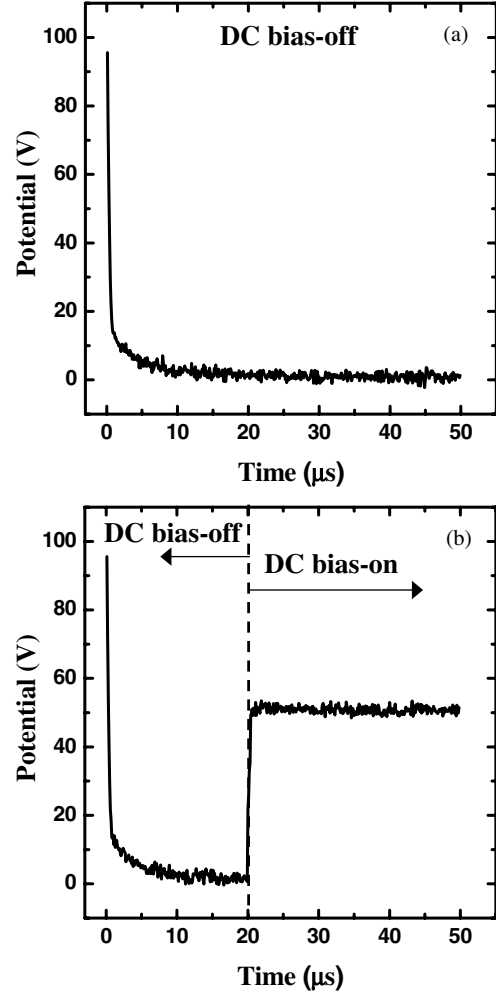


**Figure 6.** Plasma potential at the reactor centre in the afterglow, with no bias applied (a) and with a 50 V dc bias applied 20  $\mu\text{s}$  into the afterglow (b).

are accelerated by a one-dimensional (vertical) field through most of the sheath. Ions see a horizontal component of the field near the hole entrance, but the vertical ion momentum is too high to divert ions from their path. Hence the angular distribution of extracted ions is very narrow as shown in figure 9. In fact, as the applied dc bias voltage increases, the angular spread decreases as the vertical velocity component of ions becomes greater. The half width at half maximum of the distribution is only  $0.25^\circ$  at 100 V applied dc bias in the afterglow.

The predicted ion energy distribution is shown in figure 10(a). A nearly mono-energetic ion beam is obtained with energy controlled by the applied dc bias. The width of the ion energy distribution (IED) increases from 1.1 eV at 30 V dc bias to 2.9 eV at 100 V dc bias. This is due to slight gradients in the plasma potential. The small tail on the left of the IEDs is due to infrequent charge exchange collisions of ions with neutrals. The corresponding experimental data [15] are shown in figure 10(b). Good agreement with the simulation results is obtained, except that the width of the experimental IEDs is a bit larger than predicted, probably due to the finite resolution of the gridded ion energy analyzer used for measurements.

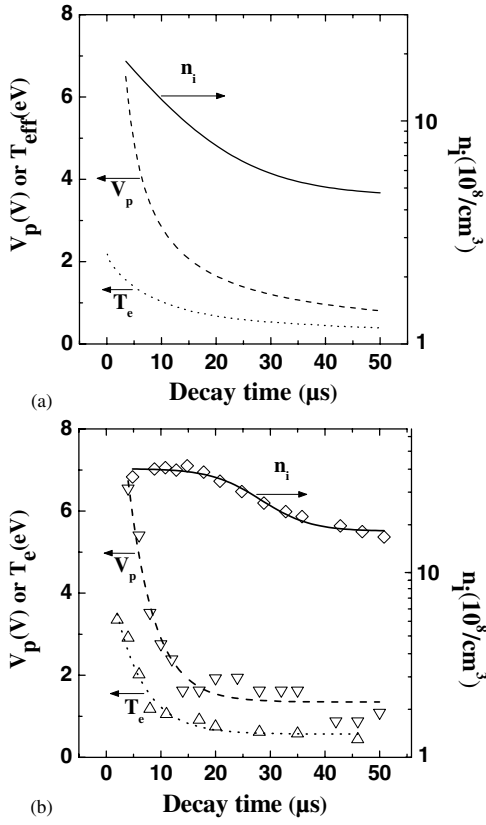


**Figure 7.** Ar ion density, electron temperature and potential at the reactor centre in the afterglow, with no bias applied, as predicted by the simulation (a) and measured by a Langmuir probe in [15] (b).

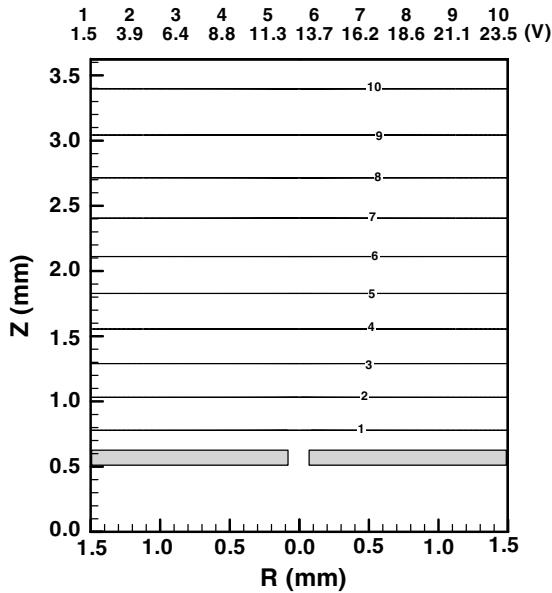


**Figure 8.** Potential distribution around a grid hole, 45  $\mu$ s into the afterglow, for 50 V dc applied 20  $\mu$ s into the afterglow. Ion flow was from top to bottom through the 142  $\mu$  diameter hole in a 127  $\mu$  thick solid grounded wall (represented by the grey area). Values of potential corresponding to contours numbered 1–10 are shown at the top.

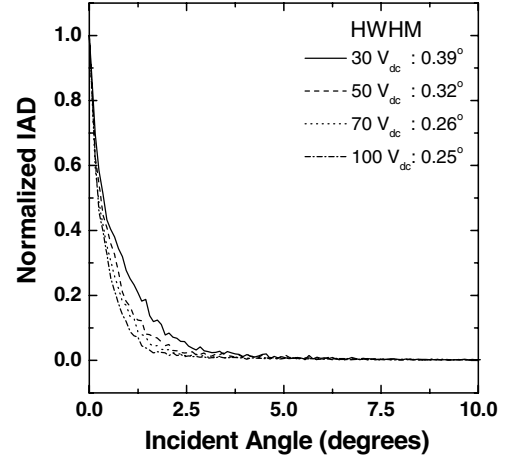


**Figure 9.** Angular distribution of extracted ions for different dc bias potentials (30, 50, 70 and 100 V) applied in the afterglow (RF power off). The bias was applied starting at 20  $\mu$ s into the afterglow. Ions were collected for the time window of 25 to 50  $\mu$ s in the afterglow (HWHM=half width at half maximum).

### 3.3. Generation of a nearly mono-energetic neutral beam

A set of neutralizer plates may be used to neutralize the extracted ion beam (figure 1) and create a fast neutral beam [24–26]. After exiting the extraction grid, ions were followed through the neutralization plates. The fast neutrals thus generated were tracked by a Monte Carlo simulation. A set of five plates separated from each other by 0.1 cm were used at a distance of 0.8 cm from the extraction grid (distance between the grid and the plane touching the top of the plates). The length of each plate was 1.0 cm. The plates were assumed to be in a differentially pumped downstream chamber of low enough background pressure so that particle flow is collision-free. Ions that encounter the solid wall are assumed to neutralize with 100% probability [14]. Ions would neutralize by, for example, an Auger process, a distance of the order of  $\sim 1$  Å from the surface. A simple surface interaction model was used, assuming specular scattering with an energy exchange given by [27]:

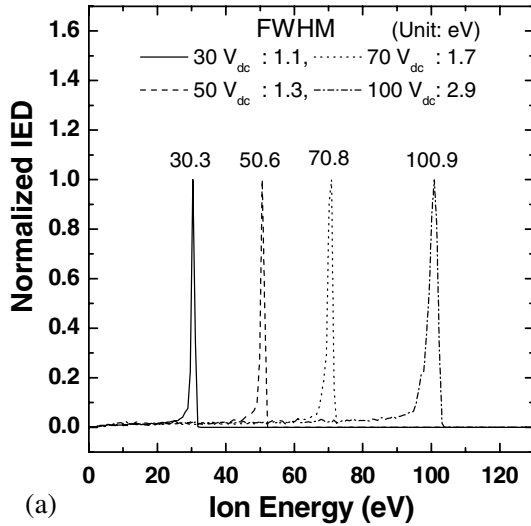
$$\sqrt{\frac{\varepsilon_r}{\varepsilon_i}} = \left( \frac{\mu}{\mu + 1} \right)^2 \left( \cos \chi_{1/2} + \sqrt{\frac{1}{\mu^2} - \sin^2 \chi_{1/2}} \right)^2, \quad (2)$$

$$\chi_{1/2} = \frac{\pi}{2} - \theta_i, \quad \mu = \frac{m_{\text{Ar}}}{m_{\text{wall}}}.$$

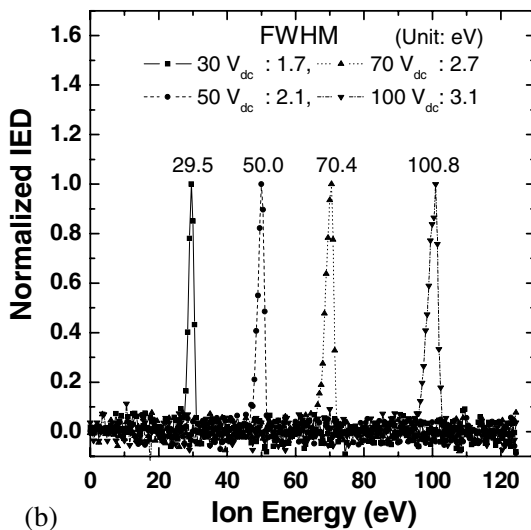
Here  $\varepsilon_i$  and  $\varepsilon_r$  are the kinetic energy of the incident and reflected atom, respectively,  $\theta_i$  is the incident angle and  $m_{\text{Ar}}$  and  $m_{\text{wall}}$  are the mass of the argon atom and the wall material atom, respectively.

This expression corresponds to two successive binary collisions of the impinging ion (actually a neutral by the time it encounters the surface) with surface atoms. Specular scattering may be a reasonable approximation for grazing angle collisions with atomically flat surfaces. However, it is expected to be a poor approximation for non-grazing angle collisions especially off real (rough) surfaces.

Figure 11 shows the fast neutral energy distribution (a) and the fast neutral angular distribution (b), for a nominal ion beam energy of 50 eV (50 V dc bias applied in the afterglow). The



(a)



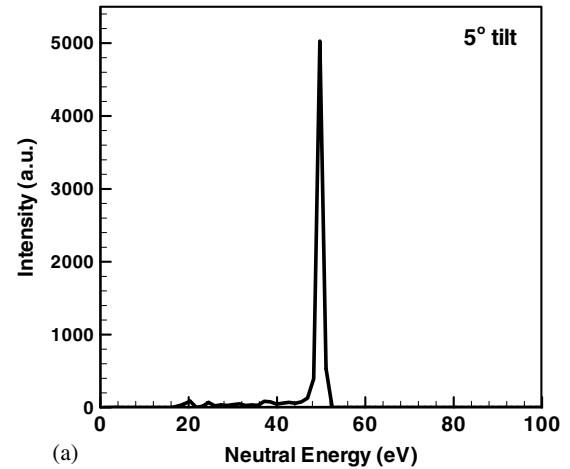
(b)

**Figure 10.** (a) Energy distribution of extracted ions for different dc bias potentials (30, 50, 70, and 100 V) applied in the afterglow (RF power off). The bias was applied starting at  $20 \mu\text{s}$  into the afterglow. Ions were collected for the time window of 25 to  $50 \mu\text{s}$  in the afterglow. (b) Experimental data of [15] for the same conditions as in the simulation (FWHM=full width at half maximum).

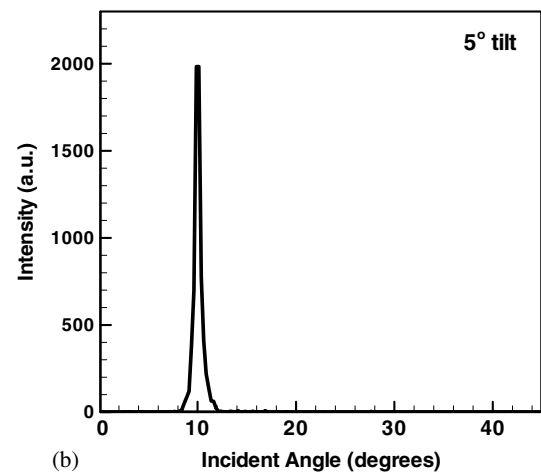
neutralization plate tilt angle was  $5^\circ$  off normal yielding a fast neutral beam at around  $10^\circ$  off normal. It appears that tilting the wafer (or other workpiece) by  $10^\circ$  would make the fast neutral beam strike perpendicular to the wafer. Importantly, the fast neutral beam is quite mono-energetic and directional. This is because of the high quality of the starting ion beam. In addition, ion neutralization occurs at grazing angles of incidence, preserving most of the parent ion kinetic energy and making specular reflection more likely (for atomically smooth surfaces).

#### 4. Summary and conclusions

A particle-in-cell simulation with Monte Carlo collisions (PIC-MC) was developed to study ion extraction from a capacitively-coupled argon plasma through a grid. A one-dimensional simulation of a plasma reactor was coupled with



(a)



(b)

**Figure 11.** Energy distribution (a) and angular distribution (b) of fast neutrals. An ion beam extracted with a dc bias of 50 V in the afterglow was neutralized by a set of 5 parallel plates separated by 0.1 cm from one another, placed 0.8 cm downstream of the extraction grid, in a chamber of low enough pressure so that particle flow is collisionless.

a two-dimensional simulation of the sheath region over a grid hole. By using a pulsed radio frequency source to power the plasma and applying a dc bias voltage during the power OFF (afterglow) fraction of the cycle, the plasma potential, and thus the ion energy, was precisely controlled. Spatial gradients in plasma potential were minimized in the afterglow, due to collapse of the electron temperature, enabling the extraction of a highly directional, nearly mono-energetic ion beam. The beam energy was set by the applied dc bias voltage. For dc bias voltages of up to 100 V, the decay of the plasma in the afterglow was not disturbed, in the sense that the electron density and temperature decay were identical to those with no applied bias in the afterglow. Simulation predictions of ion energy distributions were in good quantitative agreement with experimental measurements. The extracted ion beam could be neutralized by grazing angle collisions on a set of parallel neutralization plates downstream of the extraction grid. The resulting fast neutral beam was also quite mono-energetic and directional because, at grazing angle of incidence, most of the parent ion kinetic energy is preserved and specular reflection off an atomically smooth surface is more likely. Directional and mono-energetic ion beams are essential for

nano-pantography, a massively parallel technique to form nanometer-sized patterns of arbitrary shape over large area wafers. Directional and mono-energetic ion and neutral beams are also useful for a variety of materials processing applications including etching of fine patterns in thin films.

## Acknowledgments

The National Science Foundation (CTS 0072854 and MRI-0303790) and the Texas Advanced Technology Program are gratefully acknowledged for the financial support. SKN thanks Dr J P Verboncoeur of UC Berkeley for useful discussions concerning PIC.

## References

- [1] Rossnagel S M, Cuomo J J and Westwood W D (ed) 1990 *Handbook of Plasma Processing Technology* (Park Ridge, NJ: Noyes Publications)
- [2] Xu L, Vemula S C, Jain M, Nam S K, Donnelly V M, Economou D J and Ruchhoeft P 2005 *Nano Lett.* **5** 2563
- [3] Edelberg E A, Perry A, Benjamin N and Aydil E S 1999 *Rev. Sci. Instrum.* **70** 2689
- [4] Abraham I C, Woodworth J R, Riley M E, Miller P A, Hamilton T W and Aragon B P 2002 *J. Vac. Sci. Technol. A* **20** 1759
- [5] Miller P A and Riley M E 1997 *J. Appl. Phys.* **82** 3689
- [6] Panagopoulos T and Economou D J 1999 *J. Appl. Phys.* **85** 3435
- [7] Edelberg E A, Perry A, Benjamin N and Aydil E S 1999 *J. Vac. Sci. Technol. A* **17** 506
- [8] Wang S-B and Wendt A E 2000 *J. Appl. Phys.* **88** 643
- [9] Agarwal A and Kushner M J 2005 *J. Vac. Sci. Technol. A* **23** 1440
- [10] Coburn J W and Kay E 1972 *J. Appl. Phys.* **43** 4965
- [11] Smith B A and Overzet L J 1997 *Appl. Phys. Lett.* **70** 1980
- [12] Panda S, Economou D J and Chen L 2001 *J. Vac. Sci. Technol. A* **19** 398
- [13] Samukawa S, Sakamoto K and Ichiki K 2002 *J. Vac. Sci. Technol. A* **20** 1566
- [14] Lieberman M A and Lichtenberg A J 1994 *Principles of Plasma Discharges and Materials Processing* (New York: Wiley)
- [15] Xu L, Economou D J, Donnelly V M and Ruchhoeft P 2005 *Appl. Phys. Lett.* **87** 041502
- [16] Phelps A V and Petrović Z Lj 1999 *Plasma Sources Sci. Technol.* **8** R21
- [17] Birdsall C K 1991 *IEEE Trans. Plasma Sci.* **19** 65
- [18] Verboncoeur J P 2001 *J. Comp. Phys.* **174** 421
- [19] Vahedi V and Surendra M 1995 *Comput. Phys. Commun.* **87** 179
- [20] Nanbu K 2000 *IEEE Trans. Plasma Sci.* **28** 971
- [21] Bird G A, 1994 *Molecular Gas Dynamics and the Direct Simulation of Gas Flows* (Oxford: Clarendon)
- [22] Godyak V A, Piejak R B and Alexandrovich B M 1992 *Plasma Sources Sci. Technol.* **1** 36
- [23] Schweigert I V and Schweigert V A 2004 *Plasma Sources Sci. Technol.* **13** 315
- [24] Kim D and Economou D J 2002 *IEEE Trans. Plasma Sci.* **30** 2048
- [25] Nam S K, Economou D J and Donnelly V M 2006 *J. Phys. D: Appl. Phys.* **39** 3994
- [26] Kim D and Economou D J 2003 *J. Vac. Sci. Technol. B* **21** 1248
- [27] Kim S J, Lee H J, Yeom G Y and Lee J K 2004 *Japan. J. Appl. Phys.* **43** 7261
- [28] Nichols C A and Manos D M 1996 *J. Appl. Phys.* **80** 2643
- [29] Cuthbertson J W, Motley R W and Langer W D 1992 *Rev. Sci. Instrum.* **63** 5279
- [30] Helmer B A and Graves D B 1998 *J. Vac. Sci. Technol. A* **16** 3502